Thermal admittance spectroscopy of Mg-doped GaN Schottky diodes

N. D. Nguyen,[a] M. Germain, and M. Schmeits
Institut de Physique, Université de Liège, B5, B-4000 Liège, Belgium

B. Schineller and M. Heuken[b]
AIXTRON AG, D-52072 Aachen, Germany

Thermal admittance spectroscopy measurements at temperatures ranging from room temperature to 90 K are performed on Schottky structures based on Mg-doped GaN layers grown by metalorganic vapor phase epitaxy on sapphire. The analysis of the experimental data is made by a detailed theoretical study of the steady-state and small-signal electrical characteristics of the structures. Numerical simulations are based on the solution of the basic semiconductor equations for the structure consisting of two Schottky diodes connected back to back by a conduction channel formed by the GaN layer. The description explicitly includes the Mg-related acceptor level, with its temperature- and position-dependent incomplete occupation state, leading to a dynamic exchange with the valence band. It fully reproduces the variations with temperature of the capacitance–frequency and conductance over frequency curves, allowing to give for all temperature ranges the origin of the various contributions to the junction capacitance and of the microscopic mechanisms responsible for the capacitance–frequency cutoff. Series resistance effects are shown to be dominant at temperatures above 230 K, whereas the Mg-related acceptor level governs the electrical behavior below 230 K. The existence of a second acceptor level with an activation energy of several tens of meV is revealed from the analysis of the characteristics at low temperature. An optimized fitting procedure based on the comparison of the electrical characteristics obtained from the numerical simulations to the experimental data allows one to determine the microscopic parameters describing the structure, among which the acceptor activation energies, thermal capture cross sections, concentrations, and the Schottky contact barrier heights are the most important ones. The obtained activation energy of the Mg-acceptor level of 210 meV is by a factor of 2 larger than that obtained from a classical Arrhenius plot, showing that a complete description of Mg-doped GaN junctions requires the correct treatment of the Mg level, acting as a dopant and as deep impurity, as well as the inclusion of series resistance effects. © *2001 American Institute of Physics.*
[DOI: 10.1063/1.1379345]

I. INTRODUCTION

Gallium nitride (GaN) is a refractory III–V compound whose direct energy gap is 3.45 eV at room temperature. Together with its alloys and heterostructures, it makes GaN a well-suited component for optoelectronic applications in the UV-blue light emitting region and for high-power and high-temperature electronics. The basic properties and applications of GaN have been reviewed recently by Pearton *et al.*[1]

A major breakthrough in the realization of blue light-emitting diodes (LEDs) and lasers was achieved when *p* doping was made possible using Mg as an acceptor, *n* doping being performed with Si as a donor dopant.

The activation energy of the acceptor level related to the magnesium atoms has been measured by various experimental techniques leading to values between 70 and 250 meV,[2–14] which is much larger than for the impurities generally used as shallow dopants. As a consequence, Mg is not fully ionized at any temperature, and the resulting hole concentration is strongly temperature dependent. Furthermore,

Mg has some behaviors in common with deep impurities, leading to typical features in the electrical characteristics of *p-n* or metal–semiconductor junctions.

The electrical characteristics of GaN *p-n* junctions or of GaN Schottky diodes either of *n* or *p* type have been studied by several authors.[2–4,15–19] One interest of electrical studies is to confirm the presence of the Mg dopants and their electrical activity, and to deduce microscopic parameters such as ionization energies, capture cross sections, spatial concentration profiles, etc. Another interest is to contribute to the basic understanding of the conduction mechanism in these structures as the performances of the various electronic and optoelectronic devices depend on the efficiency of the current injection and of the carrier generation or carrier recombination. Schottky-type junctions are indeed building blocks of devices such as UV photodiodes or metal–semiconductor–metal photodetectors.[20,21]

In this work, we present results of a theoretical and experimental study of Mg-doped GaN Schottky structures. The experimentally obtained admittance curves are shown for temperatures ranging between room temperature (RT) and 90 K. The first objective of the theoretical part is to give a complete physical interpretation of the experimental results,

[a] Electronic mail: nd.nguyen@ulg.ac.be
[b] Also at: Institut f. Halbleitertechnik, RWTH Aachen, D-52056 Aachen, Germany.

i.e., to show what the basic contributions are to the capacitances at a given temperature and frequency. Variations in the frequency response manifest as cutoff frequencies in the capacitance–frequency ($C-f$) curves or as peaks in the conductance over frequency response. To determine which microscopic mechanism is responsible for each cutoff mechanism is a second objective.

Admittance spectroscopy is frequently used to characterize deep impurities in semiconductors. It indeed gives direct access to the emission–capture processes occurring between an impurity level and the conduction or the valence band. A defect state in the band gap leads to a peak in the curves of conductance over frequency, versus the frequency. Through the temperature dependence of the position of this peak, the energy activation level can in principle be deduced from an Arrhenius plot. In the case of Mg-doped GaN structures however, discrepancies between the values obtained by admittance spectroscopy and those obtained either by Hall measurements or by optical means are observed.[4] In particular, it will be shown that the direct application in admittance spectroscopy of the Arrhenius plot to determine the Mg-activation energy leads to an underestimation of this energy. Furthermore, typical features in the temperature-dependent characteristics can only be explained by the complete electrical analysis of the structure where the series resistance plays an important role. The low-temperature characteristics suggest the existence of a second shallow acceptor level with an activation energy of several tens of meV. Inclusion of several acceptor or donor levels in the used formal description is straightforward, at the expense however of an increased number of equations to be solved numerically.

The paper is organized as follows. Sec. II shows $C-f$ and conductance divided by frequency versus frequency curves at various temperatures. In Sec. III, a numerical analysis is made on the steady-state and small-signal electrical characteristics of the same structure, where the Mg-related acceptor level is explicitly included, with its position-dependent incomplete occupation state, leading to dynamic exchanges with the valence band. The aim is to fully explain the experimentally obtained electrical characteristics and, in a second stage, to obtain the values of the basic parameters corresponding to the metal–semiconductor junction with its dopant and defect distribution.

II. EXPERIMENT

A. Sample preparation and measurement procedure

The GaN layers were grown in an AIX 200RF metalorganic chemical vapor deposition (MOCVD) system using triethylgallium (TEGa), ammonia, and bis-cyclopentadienyl magnesium (Cp_2Mg) with H_2 as a carrier gas. The deposition temperature was 1120 °C. The layers consist of a nucleation layer grown directly on top of the sapphire substrate, followed by an undoped buffer layer whose thickness is about 1 μm. The latter is followed by the Mg-doped layer, which is 2 μm thick. The Cp_2Mg/TEGa gas phase ratio which determines the amount of Mg atoms incorporated is around 0.1%. The samples were annealed for 15 min at 750 °C. Two metallic contacts were evaporated on top of the
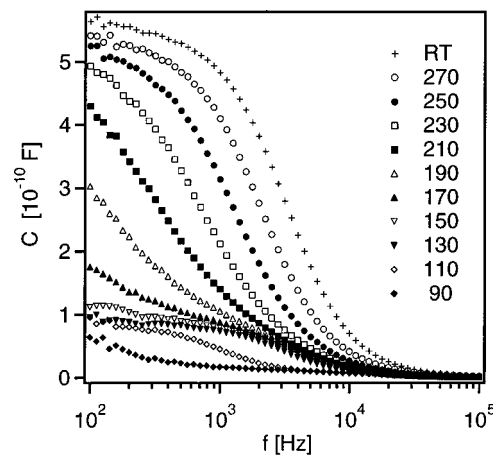

FIG. 1. Experimental ($C-f$) curves for temperatures T (K) between RT and 90 K are shown. Steady-state applied voltage is $V_0 = 0$ V.

upper GaN layers consisting of 10 nm Ni/120 nm Au. The diameter of the nonannealed contacts is about 0.5 mm and they are 2 mm apart from each other.

The impedance and the admittance of the structures were determined with a Hewlett-Packard 4192A LF impedance analyzer, for frequencies in the range of 100 Hz to 1 MHz and for positive and negative bias voltages. In the following, only results for zero bias voltage will be shown. The temperature range of investigation was from RT (293 K) down to 90 K. Current–voltage ($I-V$) measurements at different temperatures show that the contacts are of the Schottky-type. The ac measurements therefore yield the electrical characteristics of a structure consisting of two coplanar Schottky diodes, connected back to back, with the Mg-doped GaN layer as a conduction channel. The experimental curves correspond to a typical sample, results for other contacts realized on the same substrate show similar typical features.

B. Experimental admittance curves

We show in Fig. 1, the ($C-f$) curves for temperatures ranging from RT down to 90 K, for frequencies between 10^2 and 10^5 Hz and for zero bias voltage. The $C-f$ curves for the five highest temperatures show the same behavior. After a constant low-frequency capacitance value which is of 56 nF for RT conditions, the capacitance decreases down to a low value in the pF range. At RT, the cutoff frequency f_c is of 3.5 kHz, it decreases when the temperature decreases. At 210 K, the shape of the $C-f$ curves changes, leading for the lowest temperatures to a new plateau with a value of the capacitance C around 8 nF, followed by a decreasing value of the capacitance to which corresponds at 150 K a cutoff frequency of 4 kHz. When further decreasing the temperature, the cutoff frequency moves towards lower frequency values.

In Fig. 2, we show the results for the conductance G divided by $\omega = 2\pi f$, where f is the measurement frequency. For the five highest temperatures the G/ω curves show a large peak centered at the cutoff frequencies of the previously shown $C-f$ curves. The amplitude of this peak decreases with decreasing temperature. Below 230 K, a shoul-
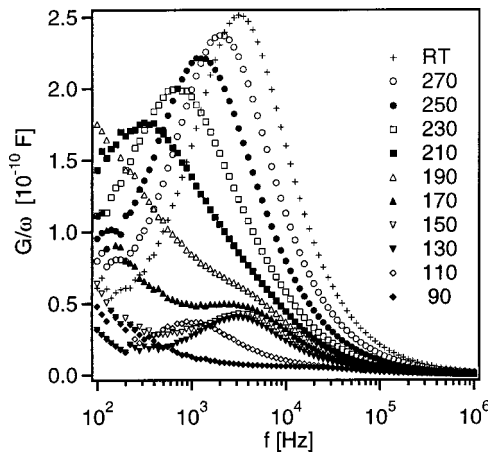
FIG. 2. Experimental curves of conductance G divided by $\omega = 2\pi f$ as function of frequency f for temperatures T (K) between RT and 90 K are shown. Steady-state applied voltage is $V_0 = 0$ V.
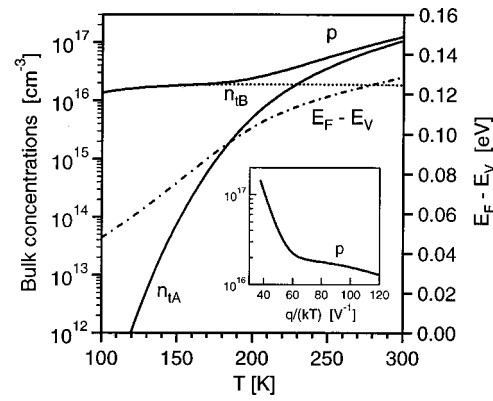

FIG. 3. Position of bulk thermal equilibrium Fermi energy E_F with respect to the valence band edge E_V, thermal equilibrium values of the hole concentration p, the level A occupation n_{tA} and the level B occupation n_{tB} as function of temperature are shown. The total concentrations of the levels are, respectively, $N_{tA} = 1 \times 10^{19}$ and $N_{tB} = 2 \times 10^{16}$ cm^{-3} and their energies relative to the valence band edge are $E_{tA} = 210$ and $E_{tB} = 30$ meV. The inset shows p as function of inverse thermal voltage q/kT.

der appears progressively on the high-frequency side of the G/ω response. The shoulder leads to a distinct peak for temperatures below 170 K. It is centered around 4 kHz for temperatures around 130 K, moving progressively to lower frequencies, when the temperature decreases.

At this stage, it would be tempting to directly use the peak positions f_c of the G/ω curves for the 200 K–RT temperature range to deduce the acceptor activation energy from an Arrhenius plot. As the theoretical analysis will show, a linear correlation of f_c/T^2 as function of the inverse temperature $1/T$ may be accidental and does not return the input value of the activation energy. Due to its relatively large activation energy, Mg acts simultaneously as a dopant and deep impurity. This complex behavior has to be introduced in the theoretical analysis, as it may lead to a competition between these two functions, the resulting characteristics depending on temperature and frequency.

Furthermore, the appearance of the low-temperature peak and its temperature dependence require the existence of a complementary mechanism, the Mg-related acceptor level determines the electrical characteristics above 200 K but cannot be related to the low-temperature results. Our interpretation will show that the introduction of a second acceptor level with an activation energy of several tens of meV can effectively explain the low-temperature admittance results.

III. THEORETICAL ANALYSIS

A. Bulk carrier concentrations

To completely describe the system, one needs the parameters corresponding to the semiconducting material, the junctions, and the fixed experimental conditions. GaN is a semiconductor whose direct gap is 3.45 eV at RT. Magnesium is known as an acceptor, with however a relatively large ionization energy, whose value in the literature is mostly given at energies of 100 to 250 meV above the valence band edge E_V. This energy position will be labeled E_{tA} and the corresponding total concentration N_{tA}. As suggested by the experimental characteristics at low temperatures, a second acceptor state could be present. It will be taken into account in

the numerical analysis with its corresponding energy position E_{tB} and concentration N_{tB}. The occupied level A concentration is given by

$$n_{tA} = \frac{N_{tA}}{1 + g \exp[(E_{tA} - E_F)/kT]}, \qquad (1)$$

where E_F is the thermal equilibrium Fermi energy, and g the degeneracy factor taken equal to 4. A similar expression holds for the occupied level B concentration n_{tB}. The thermal equilibrium hole concentration p depends on temperature T according to

$$p = N_V \exp[(E_V - E_F)/kT], \qquad (2)$$

where N_V is the effective valence band density of states. The electron concentration n expresses similarly. The charge neutrality condition is written, including eventually present fully ionized donor and acceptor concentrations N_D and N_A,

$$p - n + N_D - N_A - n_{tA} - n_{tB} = 0. \qquad (3)$$

From this relation, the equilibrium Fermi energy E_F can be obtained numerically. As an application, we show results for $(E_{tA} - E_V) = 210$ meV, $(E_{tB} - E_V) = 30$ meV, $N_{tA} = 1 \times 10^{19}$ cm^{-3}, $N_{tB} = 2 \times 10^{16}$ cm^{-3}, $N_A = N_D = 0$. In Fig. 3, we show as a function of temperature T, the resulting position of the Fermi energy E_F, the hole concentration p, and the occupied level concentrations n_{tA} and n_{tB}. The position of the Fermi energy E_F increases with increasing temperature T, keeping a position intermediate between the two defect energies E_{tA} and E_{tB}. The carrier concentrations n_{tA} and n_{tB} vary accordingly, with a resulting value of n_{tB} nearly constant above 160 K, close to N_{tB}. For these temperatures, the level B behaves as a shallow dopant, when it is considered as fully ionized. The resulting hole concentration is the sum of the contributions provided by the two acceptor levels. Below 140 K, it is essentially the shallowest level B which contributes to the hole concentration and above 200 K, the contribution of the level A is the dominant one, due to its larger

total concentration. At RT, p is equal to $1 \times 10^{17}\,\text{cm}^{-3}$, which corresponds to about 1% of ionized impurities of type A. The inset of Fig. 3 shows the plot of the hole concentration p as function of inverse thermal voltage q/kT. The variation is similar to that which is observed experimentally for $p(1/T)$ plots obtained from temperature-dependent Hall measurements.[4–9] The experimental curves effectively show above 220 K a regime with an exponential dependence of p as function of $1/T$, and a rather flat behavior for lower temperatures. In our calculations, this latter feature results from the presence of the level B concentration.

B. Basic equations and numerical procedure

The structure on which the measurements have been performed corresponds to a pair of Schottky diodes connected back to back with the GaN layer as a conducting channel. This complete system is treated in the theoretical analysis based on the resolution of the classical semiconductor equations for the free carrier and occupied level concentrations. For the acceptor concentrations considered here and due to the large value of the gap of GaN, the electron concentration n is several orders of magnitude smaller than the other concentrations and its contribution in the various equations can be neglected. The basic equations involve as unknowns the electrical potential ψ, the hole concentration p, and the level concentrations n_{tA} and n_{tB}. In the numerical study, the system is considered as one-dimensional, with x giving the position. The first equation is Poisson's equation

$$\nabla \cdot (\epsilon \nabla \psi) = -q\,(p + N_D - N_A - n_{tA} - n_{tB}), \tag{4}$$

where ϵ is the dielectric constant and $-q$ the electronic charge. The continuity equation for the holes reads

$$\frac{\partial p}{\partial t} = -\frac{1}{q}\nabla \cdot \mathbf{J}_p - r_{ptA} - r_{ptB}. \tag{5}$$

Here $\mathbf{J}_p$ is the hole current density, which is the sum of the drift and diffusion terms

$$\mathbf{J}_p = p\,\mu_p\,\nabla E_V - \mu_p\,kT\,\nabla p, \tag{6}$$

where μ_p is the hole mobility. The terms r_{ptA} and r_{ptB} represent the electron transition rates between the levels A and B and the valence band. According to the Shockley–Read–Hall scheme[22] these transition rates are written, for the case of level A

$$r_{ptA}(E_{tA}) = c_{pA}\,p\,n_{tA} - e_{pA}(N_{tA} - n_{tA}), \tag{7}$$

where c_{pA} is the capture rate for holes, expressed in terms of the hole thermal velocity v_{th}^p and the hole thermal capture cross section σ_{pA} by

$$c_{pA} = v_{th}^p\,\sigma_{pA}. \tag{8}$$

The thermal emission rate e_{pA} is given by

$$e_{pA} = \frac{c_{pA}}{g}\,N_V\,\exp[(E_V - E_{tA})/kT]. \tag{9}$$

Similar expressions hold for the transition rates to level B.

The continuity equations for the occupied concentrations of levels A and B are, respectively

$$\frac{\partial n_{tA}}{\partial t} = -r_{ptA}, \qquad \frac{\partial n_{tB}}{\partial t} = -r_{ptB}. \tag{10}$$

Under steady-state conditions, the left-hand side of Eqs. (5) and (10) is equal to zero. In the small signal analysis, the applied voltage contains, in addition to the steady-state value V_0, a sinusoidally modulated term of frequency $f = \omega/2\pi$ and of amplitude $\tilde{V}$, small with respect to kT/q

$$V = V_0 + \tilde{V}\,e^{i\omega t}. \tag{11}$$

In the small-signal analysis, all quantities will have a dc component which will be given with an index "0" and a harmonic component whose amplitude, labeled with a tilde, is complex in the general case. For example, the hole concentration writes

$$p(x,t) = p_0(x) + \tilde{p}(x)e^{i\omega t}. \tag{12}$$

Explicit expressions for the detailed developments are given in Refs. 23 and 24. The position of the left-hand side and right-hand side boundaries of the region occupied by the semiconducting material are, respectively, x_L and x_R.

We place the Schottky contacts at $x = x_L$ and x_R. In the boundary conditions, the Schottky barrier height $q\phi_b$ is fixed. In thermal equilibrium, it is related to the built-in potential V_{bi} and the bulk separation between the Fermi energy E_F and the valence band edge E_V by[25]

$$q\phi_b = qV_{bi} + (E_F - E_V). \tag{13}$$

In addition, a finite surface recombination velocity has to be given to fully characterize the metal–semiconductor contact.[26]

Instead of using the variables ψ, n, p, and n_t, the equations are expressed in terms of ψ and the quasi-Fermi energies F_p, F_{tA} and F_{tB}, as these are more appropriate, giving variations of the same order of magnitude for the four unknowns. The set of Eqs. (4)–(10) is then solved numerically, after scaling and discretization according to a variable size mesh. As results, one obtains the steady-state and small-signal values of the electrical potential ψ, the concentrations p, n_{tA}, n_{tB}, the recombination rates r_{ptA} and r_{ptB}, the current density J_p, and the displacement current J_D, in the ac case. The total ac current density $\tilde{J}$ is constant with respect to x. From its value, one obtains the admittance $Y = \tilde{J}/\tilde{V}$, from which the total capacitance C and conductance G can be obtained

$$Y = G + i\omega C. \tag{14}$$

In this expression G an C are the equivalent parallel capacitance and conductance of the whole structure. Both G and C depend on the frequency f, the steady-state voltage V_0, and the temperature T.

C. Microscopic description of the junction

Various results will be given in order to illustrate in the steady-state and small-signal case, typical space- and frequency-dependent basic features. They correspond to the aforementioned parameters for the acceptor level energies and their concentrations. In addition, the thermal capture
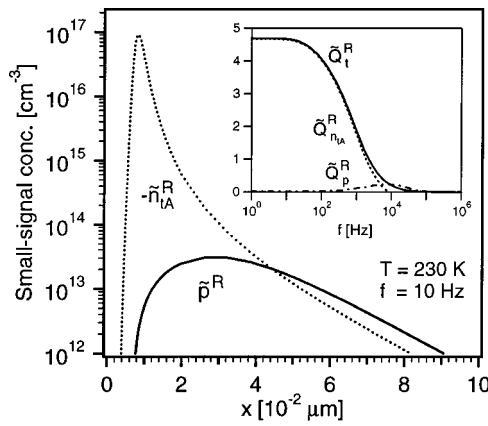
FIG. 4. Real part of small-signal amplitudes at the left contact ($x=0$) for hole concentration p, occupied level A concentration n_{tA}, at temperature $T=230$ K, and for frequency $f=10$ Hz are shown. The small-signal amplitude of occupied level B concentration is too low to appear in this plot. Inset: Integrated modulated charge per unit section (in 10^{-9} C/cm^2) as function of frequency f, due to hole concentration p, level A, level B (nearly zero), and total charge density ρ, at $T=230$ K and zero steady-state applied voltage.

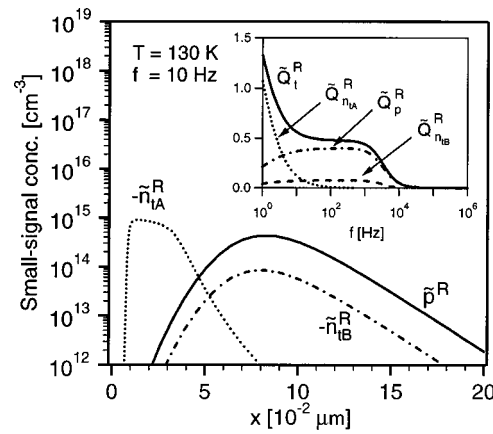FIG. 5. Real part of small-signal amplitudes at the left-hand side contact ($x=0$) for hole concentration p, occupied level A concentration n_{tA}, occupied level B concentration n_{tB}, at temperature $T=130$ K and for frequency $f=10$ Hz are shown. Inset: Integrated modulated charge per unit section (in 10^{-9} C/cm^2) as function of frequency f, due to hole concentration p, level A, level B, and total charge density ρ, at $T=130$ K and zero steady-state applied voltage.

cross sections for both levels have been fixed at 2×10^{-19} cm^2. The hole mobility μ_p is fixed at 10 cm^2/V s above $T_0=150$ K, and given a $(T/T_0)^\alpha$ dependence below that temperature. A decrease of the hole mobility below 150 K has effectively been observed experimentally.[5–9] The exponent α is considered as an additional parameter. In case of a temperature dependence imposed by impurity scattering, it is often given with a value of the order of 3/2. The Schottky barrier height is taken 1.05 eV and the surface recombination velocity of the holes is 10^9 cm/s. It is assumed that both contacts are identical i.e., they have the same Schottky barrier height. In order to reproduce the electrical characteristics of the whole structure, one has to take into account the three-dimensional character of the real structure. The major difficulty results from the fact that the conduction channel between the two contacts is not of a constant section. Its maximum value is at the Schottky contact whose diameter is in the millimeter range. The conduction between the contacts is through the GaN layer, whose thickness is in the micrometer range. A way to adapt the one-dimensional numerical procedure to model this feature, is to introduce a multiplying factor R_μ for the carrier mobilities in the region between the two depletion regions. This factor R_μ, less than one, is of the order of the ratio between the GaN layer thickness and the contact diameter. A value of the order of $R_\mu=0.005$ can be expected. For the value of the resistance of the GaN layer, it is effectively equivalent to reduce the section of the conduction channel or to reduce the conductivity by artificially reducing the hole mobility. As will be shown, this procedure reproduces the experimental values of the series resistance of the junction.

In Fig. 4, we show the small-signal values of the hole concentration $p(x)$ and of the occupied level A concentration $n_{tA}(x)$, near the left-hand side contact, for $T=230$ K, $V_0=0$ V, and $f=10$ Hz. The real part of the ac amplitude of n_{tA}, i.e., $\tilde{n}_{tA}^R$, has its maximum at $x_A=0.01$ μm, whereas $\tilde{p}^R$ presents its maximum at $x_p=0.03$ μm. The amplitude of the

variations of the shallow defect $\tilde{n}_{tB}^R$ is much less important, at least with the chosen parameter set, therefore the related curve is not shown in Fig. 4. The same quantities are reproduced in Fig. 5 for the low-temperature case $T=130$ K. Two major differences occur as compared to the $T=230$ K results. The amplitude of $\tilde{n}_{tA}^R$ is considerably reduced, while that of the modulated hole concentration $\tilde{p}^R$ has increased and is now the leading term in the ac response. These are consequences of the temperature dependence of the bulk Fermi level position with respect to the valence band edge and of the resulting junction energy band diagram.

All quantities shown up to now depend on the external parameters temperature and frequency. In order to give a synthesis of the frequency dependence, we show in the inset of Fig. 4, for $T=230$ K and $V_0=0$ V, as a function of frequency, the integrated real part of the ac amplitudes of p, n_{tA}, n_{tB}, and of the charge density ρ. The different parts are defined as follows

$$\tilde{Q}_{n_{tA}}^R = q \int_{x_L}^{x_u} (-\tilde{n}_{tA}^R) dx, \tag{15}$$

$$\tilde{Q}_{n_{tB}}^R = q \int_{x_L}^{x_u} (-\tilde{n}_{tB}^R) dx, \tag{16}$$

$$\tilde{Q}_p^R = q \int_{x_L}^{x_u} \tilde{p}^R dx, \tag{17}$$

$$\tilde{Q}_t^R = q \int_{x_L}^{x_u} (\tilde{p}^R - \tilde{n}_{tA}^R - \tilde{n}_{tB}^R) dx, \tag{18}$$

where x_u is an upper limit of integration, sufficiently large such that the different integrands can be considered as zero beyond x_u. The charge defined by relation (18) relates to the imaginary part of the total current amplitude by

$$\tilde{J}^I = \omega \tilde{Q}_t^R. \tag{19}$$

The inset of Fig. 4 shows that the response of the level A and the hole concentration is constant up to 10^2 Hz. Beyond this value, the amplitude of the level A response decreases, as the defect level is no longer able to follow the applied voltage modulation. The mean frequency of the decreasing response is 3×10^3 Hz. The response of the level B is negligible in that temperature range. The hole amplitude, contrary to the level A response, increases above 10^2 Hz, reaches a maximum at 10^4 Hz and decreases beyond that value, a cutoff frequency for the hole response could be fixed at 2×10^4 Hz. The total charge density modulation is the resulting curve, with a cutoff frequency at 4×10^3 Hz. Dividing $\tilde{Q}_t^R$ by the voltage amplitude $\tilde{V}$ yields the frequency-dependent capacitance of the single junction, as a result from relations (14) and (19). In fact, this is a case where the $R_s C$-cutoff frequency, with R_s as the series resistance and C as the hole depletion layer capacitance is located slightly above the defect-A transition frequency f_{tA}. Therefore, the hole response cannot reach its maximum amplitude and the total cutoff frequency is practically equal to the defect transition frequency f_{tA}.[24]

In the inset of Fig. 5 we show the same quantities, but for a low-temperature case, with $T = 130$ K. The response of the level A has moved to lower frequencies, by about 3 decades. The hole amplitude modulation is maximum for $f = 3 \times 10^2$ Hz. The resulting amplitude of the integrated charge density modulation shows now a two-step behavior with a low-frequency cutoff determined by the level A response and a second cutoff above 10^3 Hz determined by the hole response. In terms of equivalent electrical circuits, the hole response is due to the modulation of the depletion layer width, whose cutoff frequency is given, in the case of a classical junction with fully ionized shallow dopants by the $R_s C$ constant of the structure, where R_s is the series resistance and C is the depletion layer capacitance.

D. Admittance curves of the back to back connected Schottky junctions

The theoretical curves are obtained with a one-dimensional system giving electrical quantities per unit section. In the following, the section will be fixed by normalization of the low-frequency value of the RT capacitance to the experimental RT capacitance value. Normalizing to the height of the main peak in the $G(\omega)/\omega$ curve would yield similar results. To analyze the resulting electrical characteristics, a series of parameters describing the structure has to be fixed. The length $(x_R - x_L)$ is taken equal to the mean distance between the two contacts. The hole effective mass is fixed at $m_p = 0.8 m_0$.[5] The parameters which remain to be determined are the Schottky barrier height $q\phi_b$ at the two junctions, the position of the two levels E_{tA} and E_{tB} and their respective concentrations N_{tA} and N_{tB}, their thermal capture cross sections σ_{pA} and σ_{pB} and the factor R_μ. The RT hole mobilty μ_p has been fixed to 10 cm^2/V s, with a $(T/T_0)^\alpha$ temperature dependence below $T_0 = 150$ K. We have not considered the mobility μ_p as an independent parameter as the reduction factor R_μ is already used. The concentrations
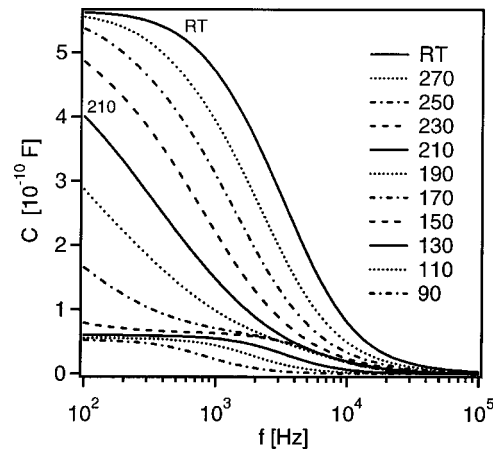

FIG. 6. Theoretical $C-f$ curves for temperatures between RT and $T = 90$ K are shown. Steady-state applied voltage is $V_0 = 0$ V.

of eventually present, other completely ionized shallow donors, N_D, and acceptors, N_A, have been set equal to zero.

The electrical characteristics are then calculated at various temperatures, starting from an initial guess with typical values as given in the literature. In the optimization procedure, a least-square fit is used to determine the open parameters such as to best reproduce the experimentally obtained G/ω curves. In a first step, the major features such as the peak positions are adjusted, a refinement in a second step corrects the complete set of temperature-dependent G/ω curves. Figure 6 gives the resulting $C-f$ curves and Fig. 7, the G/ω curves. The obtained parameters are $R_\mu = 0.007$, $\alpha = 3$, $q\phi_b = 1.05$ eV, $(E_{tA} - E_V) = 210$ meV, $(E_{tB} - E_V) = 30$ meV, $N_{tA} = 1 \times 10^{19}$ cm^{-3}, $N_{tB} = 2 \times 10^{16}$ cm^{-3}, $\sigma_{pA} = 2 \times 10^{-19}$ cm^2, and $\sigma_{pB} = 2 \times 10^{-19}$ cm^2.

First, the as-obtained parameters are compared to experimental values reported in the literature. Schottky barrier heights depend on the nature of the metal, on surface preparation conditions, and on interface oxide layers. For contacts on p-doped GaN, barrier heights are obtained from an analysis of $I-V$ characteristics and give, respectively, $q\phi_b = 0.9$ eV,[27] 1.05 eV,[19] 0.50–0.65 eV,[15] 0.49 eV,[17] even values
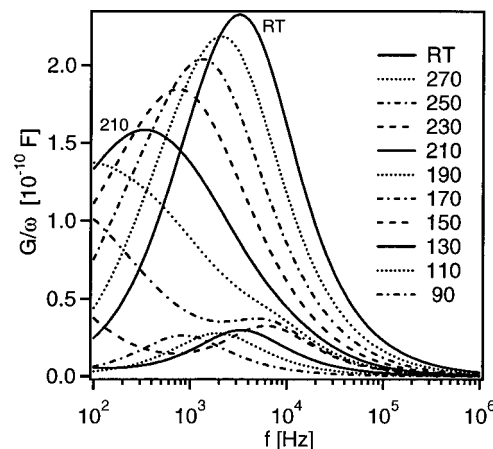

FIG. 7. Theoretical G/ω curves as a function of frequency for temperatures between RT and $T = 90$ K are shown. Steady-state applied voltage is $V_0 = 0$ V.
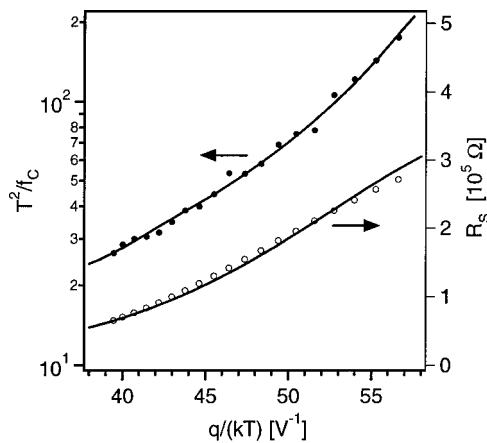
FIG. 8. Theoretical ($-$) and experimental ($\bullet$) values of T^2/f_c, with f_c the capacitance cutoff frequency (equal to the G/ω peak position) as function of the inverse thermal voltage q/kT for temperatures from $T=200$ to $T=300$ K. The second curve shows the theoretical ($-$) and experimental ($\bigcirc$) values of the series resistance R_s.
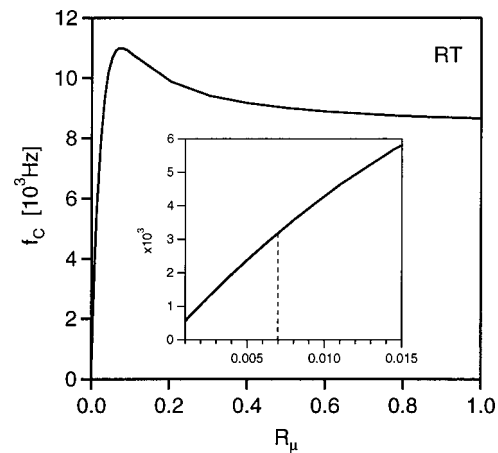

FIG. 9. Position of main peak in G/ω vs frequency curve at $T=293$ K, as function of the reduction factor R_μ is shown. The inset shows same values in the enhanced region of $R_\mu=0.001$ to 0.015. Numerical fit yields best agreement for $R_\mu=0.007$.

as high as 2.4 eV for Ni/p-GaN contacts have been mentioned.[28] The activation energy of the Mg-related acceptor level has been determined by various methods, the resulting values depend on growth method and Mg concentration. From the study of the temperature dependence of the hole concentration obtained by Hall measurements on GaN layers, values of 112 to 190 meV are given,[4–9] by admittance spectroscopy, values of 70 to 160 meV are cited.[2–4] In some cases, the value obtained by admittance measurements was lower than that obtained from the Hall method.[4] Photoluminescence studies of the donor–acceptor recombination yield again a different set of values between 150 and 250 meV.[10–14] The thermal capture cross section of the A level of 2×10^{-19} cm^2 is close to the value given by admittance spectroscopy in Ref. 4.

Several acceptor levels in the same sample have been observed experimentally.[2,5,29] Their energy positions depend on the growth method and sample preparation, but most are located at least at 100 meV above the valence band edge. In our study, their concentration N_{tB} is rather weak as compared to the value of N_{tA}, and their effect only appears at temperatures below 150 K. This may explain why acceptor levels with activation energies around 30 meV have not been detected in the past with the used experimental techniques. The thermal capture cross section for level B has been set equal to that for the level A. As will be seen from the discussion below, it is not possible to determine σ_{pB} from the electrical characteristics, as the level B influences the thermal equilibrium Fermi energy and the temperature-dependent hole concentration, but not the dynamical response to the applied modulating voltage.

The theoretically obtained temperature-dependent C–f and G/ω curves well reproduce the experimental curves shown in Figs. 1 and 2. The different regimes at high and low temperatures can be explained with the help of the above mentioned microscopic characteristics.

Above 200 K, the capacitance is due to the modulation of the space charge for which the defect state A related to the magnesium is responsible. Figure 8 gives the experimental

and theoretical value of T^2/f_c, where f_c is the peak position of G/ω in this temperature range. Good agreement between theory and experiment is obtained. The figure also shows a comparison of the experimental and theoretical value of the equivalent series resistance, which is obtained from the high-frequency value of the real part of the impedance $Z=1/Y$. At high frequency, the equivalent circuit of the whole structure reduces to the series resistance R_s as the impedance of the capacitances becomes negligible. The agreement between the experimental and theoretical values justifies the use of the reduction factor R_μ, to simulate the effect of the geometrical structure. In Fig. 9, we show for RT conditions, the theoretically obtained value of the position of the dominant peak in the G/ω curves f_c as a function of the reduction factor R_μ, for values of R_μ between 0.001 and 1. For values of R_μ above 0.4, the peak frequency remains constant, as it corresponds to the defect transition frequency. A second peak in the G/ω curves is at a higher frequency and corresponds to a RC cutoff. Below $R_\mu=0.4$, it progressively merges into the first peak, leading to a slight increase on the resulting peak frequency. Below $R_\mu=0.1$, the peak frequency decreases. As the inset of Fig. 9 shows, the variation of f_c is nearly linear in that parameter range. The frequency f_c is proportional to R_μ, i.e., inversely proportional to the series resistance R_s. This strongly indicates that the RT temperature cutoff frequency is due in fact to the electrically R_sC cutoff, where C is the low-frequency capacitance, and no more to the defect transition frequency.

An additional argument in favor of this interpretation in this temperature range is furthermore given by the results shown in Fig. 10, where the cutoff frequency position f_c is shown as function of temperature T. The lower curve gives the values of f_c for the up to now studied double Schottky structure, whereas the upper curve corresponds to a single Schottky diode with a total length of 1 μm, and $R_\mu=1$. In this latter case, no R_sC-cutoff frequency can be expected in this temperature range, f_c therefore is equal to the defect transition frequency f_{tA}. The comparison of the frequencies f_c for the two systems clearly shows the transition between
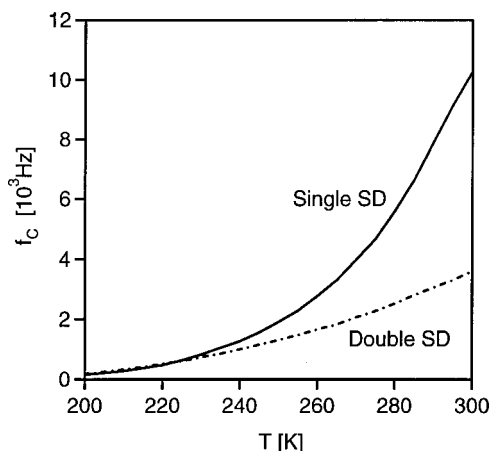
FIG. 10. Position of main peak in G/ω vs frequency curve as function of temperature T, for complete double Schottky diode structure (lower curve) and for single Schottky contact with reduced length $(x_R - x_L) = 1$ μm, $R_\mu = 1$ and otherwise identical parameter set (upper curve).

the two regimes. Above 250 K, the electrical behavior of the circuit determines the cutoff frequency. Below 230 K, it is the reduced response of the Mg-related defect state E_{tA}, which imposes the reduction of the equivalent capacitance of the structure.

As a consequence, care should been taken in attempting to directly deduce the activation energy from an Arrhenius plot. First, the system under study here consists of the Mg level, which acts simultaneously as the p dopant and deep impurity. This is a situation where the assumptions leading to the identification of the defect transition frequency f_t with the thermal emission rate are not fulfilled.[18,24,30] Even when resistance effects do not exist, this leads to an expression of f_t which is not simply equal to the hole emission rate e_p, the difference in magnitude being of the order of a factor 10–50 and the temperature dependence not simply that of a thermally-activated process. Starting with an input value of $(E_{tA} - E_V) = 210$ meV, we have determined f_{tA} by calculating the G/ω peak position for a single and sufficiently short Schottky diode, such that series resistance effects play no role. With temperatures from 200 to 300 K, the Arrhenius plot yields an activation energy of 176 meV. This apparent shift of 30–40 meV corresponds to similar values as were obtained by Kozodoy *et al.*[18] and Kim.[30] Using the values of the theoretical peak positions for the complete structure as shown in Fig. 8, one obtains an apparent linear relation in a log representation of T^2/f_c as a function of the inverse thermal voltage q/kT. The resulting activation energy is now 107 meV, which is clearly distinct from the input value 210 meV and the ideal transition frequency $f_{tA} = 176$ meV. As this discussion has shown, the cutoff frequency is the feature resulting from two cutoff mechanisms which both are present in the 200–300 K temperature range. The fact of obtaining a linear relationship in a semilog representation might therefore be, in some cases, purely fortuitous. It implicitly assumes that the temperature dependence of the transition frequency is the same as that of the thermal hole emission rate, as given by expression (9). But doing so even in the case of deep impurities, at concentrations lower than that of the shal-

low dopant, several terms given in the expression of the transition frequency are neglected.[31] This approximation is even worse in the case of Mg-doped GaN, where Mg is at an energy level which simultaneously acts as a dopant and deep impurity.

Below 200 K, the main peak in G/ω moves below the 100 Hz limit of the measurement equipment, but a shoulder appears in the $10^3 - 10^4$ Hz frequency range leading to a well-defined second peak below 170 K. With the help of Fig. 5, the following interpretation can be given to this peak. In the inset of Fig. 5, the integrated amplitudes of the small signal response of the various contributions to the charge modulation in the vicinity of the junctions are given. It is shown that the response of level A has moved to very low frequencies, below 10 Hz. The response of level B is nonzero but an order of magnitude lower than that of the holes. For this reason, it is impossible to get a precise quantitative information on the capture cross section of this shallow acceptor level. Above 10 Hz, the major contribution is due to the holes. This corresponds to the modulation of the depletion layer width in a classical p-n junction or a metal/p–semiconductor junction. This contribution remains when the deep impurity levels no longer respond to the variations of the applied voltage. The cutoff frequency is equal to $1/(2\pi R_s C)$ where R_s is again the series resistance essentially due to the conducting layer between the depletion layers and C is the combined capacitance of the two Schottky contacts. The capacitance of each contact is only weakly temperature-dependent in this temperature range, and the variation of the peak position and amplitude with temperature is mainly due to the temperature dependence of the series resistance. The RC-cutoff frequency is therefore proportional to the conductivity of the GaN layer, which means proportional to the hole concentration p and the hole mobility μ_p. As seen in Fig. 3, the hole concentration p decreases only weakly from 160 to 120 K, as does the mobility μ_p, which explains that the displacement of this peak, is small in this temperature range. Below 120 K, the reduction in temperature of the hole concentration p and of the hole mobility due to increased impurity scattering, is responsible for the lowering of the capacitance cutoff frequency and of the low-temperature peak position. The reduction of the peak height with temperature is due to the reduction of the effective hole concentration p. The appearance of this peak in the admittance curves is the combined result of the large value of the series resistance, the large distance between the contacts, the low intrinsic hole mobility of GaN and the geometry of the double Schottky structure, which is included through the reduction factor R_μ. As shown in Fig. 7, this second peak does not appear in the high-temperature curves as it is hidden by the high-frequency part of the first peak.

We have attempted to explain the existence and temperature dependence of this low-temperature peak by other effects, such as an asymmetry between the two contacts, a second level of donor type or a second acceptor level being fully ionized at all temperatures, which is equivalent to a nonzero concentration N_A. But all these models were unable to correctly reproduce the experimental results. Taking, for example, a constant value of N_A produces a low-

J. Appl. Phys., Vol. 90, No. 2, 15 July 2001

Nguyen *et al.* 993

temperature peak in the G/ω curves by the same RC-cutoff mechanism, but there is only a weak shift of this peak when the temperature decreases. This final analysis shows that only the introduction of a second acceptor state with an activation energy of about 30 meV completely explains the low-temperature electrical characteristics.

IV. CONCLUSIONS

We have determined experimental temperature-dependent admittance curves for Mg-doped GaN double Schottky diodes grown by MOCVD. The G/ω curves show in the temperature range of $T=200\text{–}300$ K a dominant peak which moves to lower frequencies with decreasing temperature. The capacitance–frequency curves have cutoff frequencies at the same values. Below 150 K, a second peak in the G/ω curves appears with its own temperature dependence.

The theoretical study is based on the numerical simulation of the complete structure with the two Schottky contacts and the hole conduction through the GaN channel between the contacts. It includes the Mg-related acceptor level at an energy position of 210 meV above the valence band edge E_V, with a total concentration of $N_{tA}=1\times10^{19}\,\text{cm}^{-3}$, as well as a second shallow acceptor state at 30 meV above E_V and a concentration of $2\times10^{16}\,\text{cm}^{-3}$. The numerical results explain the basic mechanisms responsible for the temperature dependence of the ac electrical characteristics, leading to a good agreement with the experimentally obtained values.

The analysis suggests that only a complete numerical study allows a correct interpretation of the admittance curves. In particular, the microscopic parameters can only be obtained from an optimized fit with a numerical simulation program. It is explicitly shown that deducing activation energies from an Arrhenius plot of the transition frequencies would lead in the case of the system we have studied to an underestimation of the activation energies.

This work contributes to the basic understanding of the role played by the particular dopant which is magnesium, having the functions of dopant and deep impurity simultaneously. Which role is dominant depends on the external conditions such as temperature, applied voltage or modulation frequency, and on the characteristic values of the Mg acceptor itself, mainly its energy position in the gap and its concentration. Despite the numerous works devoted to this system, many aspects remain to be explored.

The experimental aspects could be completed by studies under modified experimental conditions, such as illumination or large-signal response and by using structures which reduce to a single metal–semiconductor contact where series resistance effects could be neglected. There, only the intrinsic response of the Mg-level would contribute to the electrical signal. The numerical study could of course be applied to other configurations of interest, such as GaN-based transistors, photodetectors, and p-n junctions. The latter are the basis of LEDs. Inclusion of more than two acceptor levels, as well as donor levels in the forbidden gap or a continuous defect density of states, are also possible.

[1] S. J. Pearton, J. C. Zolper, R. J. Shul, and F. Ren, J. Appl. Phys. **86**, 1 (1999).
[2] J. W. Huang, T. F. Kuech, H. Lu, and I. Bhat, Appl. Phys. Lett. **68**, 2392 (1996).
[3] Y. Zohta, H. Kuroda, R. Nii, and S. Nakamura, J. Cryst. Growth **189**, 816 (1998).
[4] D. J. Kim, D. Y. Ryu, N. A. Bojarczuk, J. Karasinski, S. Guha, S. H. Lee, and J. H. Lee, J. Appl. Phys. **88**, 2564 (2000).
[5] T. Tanaka, A. Watanabe, H. Amano, Y. Kobayashi, I. Akasaki, S. Yamazaki, and M. Koike, Appl. Phys. Lett. **65**, 593 (1994).
[6] W. Götz, N. M. Johnson, J. Walker, D. P. Bour, and R. A. Street, Appl. Phys. Lett. **68**, 667 (1996).
[7] H. Nakayama, P. Hacke, M. R. H. Khan, T. Detchprohm, K. Hiramatsu, and N. Sawaki, Jpn. J. Appl. Phys., Part 2 **35**, L282 (1996).
[8] H. Nagai, Q. S. Zhu, Y. Kawaguchi, K. Hiramatsu, and N. Sawaki, Appl. Phys. Lett. **73**, 2024 (1998).
[9] P. Kozodoy, H. Xing, S. P. Den Baars, U. K. Mishra, A. Saxler, R. Perrin, S. Elhamri, and W. C. Mitchel, J. Appl. Phys. **87**, 1832 (2000).
[10] M. Ilegems and R. Dingle, J. Appl. Phys. **44**, 4234 (1973).
[11] J. A. Pankove and J. A. Hutchby, J. Appl. Phys. **42**, 5387 (1976).
[12] U. Kaufmann, M. Kunzer, M. Maier, H. Obloh, A. Ramakrishnan, B. Santic, and P. Schlotter, Appl. Phys. Lett. **72**, 1326 (1998).
[13] T. W. Kang, S. H. Park, H. Song, T. W. Kim, G. S. Yoon, and C. O. Kim, J. Appl. Phys. **84**, 2082 (1998).
[14] A. K. Viswanath, E. Shin, J. I. Lee, S. Yu, D. Kim, B. Kim, Y. Choi, and C. H. Hong, J. Appl. Phys. **83**, 2272 (1998).
[15] T. Mori, T. Kozawa, T. Ohwaki, Y. Taga, S. Nagai, S. Yamasaki, S. Asami, N. Shibata, and M. Koike, Appl. Phys. Lett. **69**, 3537 (1996).
[16] A. Krtschil, H. Witte, M. Lisker, J. Christen, U. Birkle, S. Einfeldt, and D. Hommel, J. Appl. Phys. **84**, 2040 (1998).
[17] X. A. Cao, S. J. Pearton, G. Dang, A. P. Zhang, F. Ren, and J. M. Van Hove, Appl. Phys. Lett. **75**, 4130 (1999).
[18] P. Kozodoy, S. P. Den Baars, and U. K. Mishra, J. Appl. Phys. **87**, 770 (2000).
[19] E. Monroy, F. Calle, J. L. Pau, F. J. Sanchez, E. Munoz, F. Omnes, B. Beaumont, and P. Gibart, J. Appl. Phys. **88**, 2081 (2000).
[20] E. Monroy, M. Hamilton, D. Walker, P. Kung, F. J. Sanchez, and M. Razeghi, Appl. Phys. Lett. **74**, 1171 (1999).
[21] Z. M. Zhao, R. L. Jiang, P. Chen, D. J. Xi, Z. Y. Luo, R. Zhang, B. Shen, Z. Z. Chen, and Y. D. Zheng, Appl. Phys. Lett. **77**, 444 (2000).
[22] W. Shockley and W. T. Read, Phys. Rev. **87**, 835 (1952); R. N. Hall, Phys. Rev. **87**, 387 (1952).
[23] M. Sakhaf and M. Schmeits, J. Appl. Phys. **80**, 6839 (1996).
[24] M. Schmeits, N. D. Nguyen, and M. Germain, J. Appl. Phys. **89**, 1890 (2001).
[25] S. M. Sze, *Physics of Semiconductor Devices* (Wiley, New York, 1981).
[26] S. Selberherr, *Analysis and Simulation of Semiconductor Devices* (Springer, Berlin, 1984).
[27] Z. Z. Bandic, P. M. Bridger, E. C. Piquette, and T. C. McGill, Appl. Phys. Lett. **73**, 3276 (1998).
[28] K. Shiojima, T. Sugahara, and S. Sakai, Appl. Phys. Lett. **74**, 1936 (1999).
[29] H. Nagai, Q. S. Zhu, Y. Kawaguchi, K. Hiramatsu, and N. Sawaki, Appl. Phys. Lett. **73**, 2024 (1998).
[30] D. J. Kim, J. Appl. Phys. **88**, 1929 (2000).
[31] W. G. Oldham and S. K. Naik, Solid-State Electron. **15**, 1085 (1972).